Journal of the Neurological Sciences 451 (2023) 120726

Contents lists available at ScienceDirect

Journal of the Neurological Sciences

journal homepage: www.elsevier.com/locate/jns

Radiological correlates of pseudobulbar affect: Corticobulbar and cerebellar components in primary lateral sclerosis

Marlene Tahedl [a,1], Ee Ling Tan [a,1], We Fong Siah [a], Jennifer C. Hengeveld [b], Mark A. Doherty [b], Russell L. McLaughlin [b], Orla Hardiman [a], Eoin Finegan [a,2], Peter Bede [a,c,*,2]

[a] Computational Neuroimaging Group (CNG), School of Medicine, Trinity College Dublin, Ireland
[b] Smurfit Institute of Genetics, Trinity College Dublin, Dublin, Ireland
[c] Department of Neurology, St James's Hospital, Dublin, Ireland

ARTICLE INFO

Keywords:
Pseudobulbar affect
Primary lateral sclerosis
Motor neuron disease
MRI
Biomarkers

ABSTRACT

Introduction: Pseudobulbar affect (PBA) is a distressing symptom of a multitude of neurological conditions affecting patients with a rage of neuroinflammatory, neurovascular and neurodegenerative conditions. It manifests in disproportionate emotional responses to minimal or no contextual stimulus. It has considerable quality of life implications and treatment can be challenging.

Methods: A prospective multimodal neuroimaging study was conducted to explore the neuroanatomical underpinnings of PBA in patients with primary lateral sclerosis (PLS). All participants underwent whole genome sequencing and screening for *C9orf72* hexanucleotide repeat expansions, a comprehensive neurological assessment, neuropsychological screening (ECAS, HADS, FrSBe) and PBA was evaluated by the emotional lability questionnaire. Structural, diffusivity and functional MRI data were systematically evaluated in whole-brain (WB) data-driven and region of interest (ROI) hypothesis-driven analyses. In ROI analyses, functional and structural corticobulbar connectivity and cerebello-medullary connectivity alterations were evaluated separately.

Results: Our data-driven whole-brain analyses revealed associations between PBA and white matter degeneration in descending corticobulbar as well as in commissural tracts. In our hypothesis-driven analyses, PBA was associated with increased right corticobulbar tract RD ($p = 0.006$) and decreased FA ($p = 0.026$). The left-hemispheric corticobulbar tract, as well as functional connectivity, showed similar tendencies. While uncorrected *p*-maps revealed both voxelwise and ROI trends for associations between PBA and cerebellar measures, these did not reach significance to unequivocally support the "cerebellar hypothesis".

Conclusions: Our data confirm associations between cortex-brainstem disconnection and the clinical severity of PBA. While our findings may be disease-specific, they are consistent with the classical cortico-medullary model of pseudobulbar affect.

1. Introduction

Pseudobulbar affect (PBA) refers to recurrent episodes of exaggerated emotional reaction to minimal external stimulus which would have not typically triggered such as response in the affected individual previously. Context-inappropriate crying or laughing are the most commonly reported symptoms, but excessive yawning is also considered to be part of the clinical spectrum of PBA. Commonly used alternative terminology includes "pathological crying and laughing (PCL)", "emotional lability (EL)", or "involuntary emotional expression disorder (IEED)" [1,2]. The sudden outbursts associated with PBA are often in line with the individual's transient emotional state [3–5], but the responses are invariably disproportionate to the stimulus and often inappropriate to the social context.

PBA has been observed in a multitude of neurological syndromes spanning from acquired brain injury to neurodegenerative conditions,

* Corresponding author at: Room 5.43, Computational Neuroimaging Group (CNG), Trinity Biomedical Sciences Institute, Trinity College Dublin, Pearse Street, Dublin 2, Ireland.
E-mail address: bedep@tcd.ie (P. Bede).
[1] Contributed equally as joint first authors.
[2] Contribute equally as joint senior authors.

https://doi.org/10.1016/j.jns.2023.120726
Received 26 April 2023; Received in revised form 2 June 2023; Accepted 28 June 2023
Available online 30 June 2023

but it is particularly common in motor neuron diseases (MND), multiple sclerosis (MS), stroke, multiple system-atrophy-cerebellar type (MSA-C), traumatic brain injury (TBI), Alzheimer's disease, and Parkinson's disease. Irrespective of the underlying aetiology, PBA has significant quality of life implications. Patients with PBA typically find the unprovoked outbursts of emotional responses very troublesome, and often chose to limit social interactions due the fear their symptoms may be misinterpreted as psychiatric or cognitive manifestations. PBA can cause considerable embarrassment, social withdrawal and has a multitude of quality of life implications. [6]

Albeit PBA has a rich and well documented literature, no single unifying pathophysiological explanation exists. While the classical view [7] on the underlying mechanism centres on impaired corticobulbar control of ingrained brainstem responses, the contribution of impaired cerebellar gaiting processes, serotonergic and frontotemporal dysfunction are increasingly recognised [5,8–14]. It may be the case that several mechanisms converge to the unique constellation of clinical symptoms referred to as PBA or that divergent aetiologies may lead to PBA in different conditions. Within the MND spectrum PBA is most commonly reported in patients with primary lateral sclerosis (PLS) or upper motor neuron-predominant amyotrophic lateral sclerosis (ALS) and not commonly observed in lower motor neuron predominant syndromes such as Kennedy's disease, progressive muscular atrophy (PMA) or adult spinal-muscular atrophy [15–24]. The study of clinically well-characterised homogenous diagnostic groups may offer unique opportunities to evaluate the neuronal underpinnings of PBA. The most widely accepted pathomechanism of PBA is brainstem-cortex disconnection, but in motor neuron diseases, cerebellar processes have also been consistently implicated [5,12–14,25]. Frontotemporal dysfunction is well characterised in ALS [26–28] and frontal lobe atrophy [12] and fronto-cerebellar connectivity alterations have been specifically linked to PBA [13].

Accordingly the overarching objective of this study is the nuanced evaluation of the radiological correlates of PBA without anatomical *a priori* hypotheses in a large cohort of clinically- and genetically well-characterised cohort of primary lateral sclerosis patients. Based on data from ALS [5,12,13], an additional objective of our study is the targeted assessment of the two most commonly proposed pathomechanisms, namely the contribution of corticobulbar and cerebellar disease-burden to PBA.

2. Methods

2.1. Standard protocol approvals, registrations, and patient consents

All participants gave informed consent in accordance with the Ethics Approval of this research study (Beaumont Hospital, Dublin, Ireland - IRB).

2.2. Participants

In a single-centre, prospective neuroimaging study, multimodal MR data from 35 patients with primary lateral sclerosis were systematically analysed (Table 1). Patients were diagnosed in accordance with the current consensus diagnostic criteria [29]. Exclusion criteria included prior neurosurgery, antecedent cerebrovascular events, preceding traumatic brain injury, established neoplastic, neuroinflammatory or psychiatric conditions. Comorbid frontotemporal dementia was not considered an exclusion criterion. Patients were screened for neuropsychological deficits and depression using the Edinburgh Cognitive and Behavioural ALS Screen (ECAS) [30], the Frontal Systems Behavior Scale (FrSBe), and the Hospital Anxiety and Depression Scale (HADS). The Emotional Lability Questionnaire (ELQ) was administered to evaluate the severity of PBA [31] and this score was used to explore the anatomical correlates of PBA. The ELQ is a 33-item questionnaire divided into three main domains; laughing, crying and smiling. Motor disability was appraised using the revised ALS functional rating scale (ALSFRS-r) which offers a composite score of disability in four main domains; bulbar, upper-limb, lower-limb and respiratory function [32]. The Edinburgh Cognitive and Behavioural Screen (ECAS) screens for cognitive impairment in language, verbal fluency, executive, memory and visuospatial domains [30] and has been thoroughly validated in the Irish population with the generation of local normative data [33]. The FrSBe evaluates apathy, disinhibition and executive dysfunction across 46 items [34].

Table 1
Demographic and clinical details of the PLS study population.

	PLS patients
Age (year) - mean ± SD]	61.06 ± 9.77
Sex - F/M	15/20
Handedness - R/L	31/4
Years of education - mean ± SD	12.97 ± 3.16
ELQ score - mean ± SD	12.34 ± 14.91
ELQ score - median, IQR	5 [0.17; 24]
Symptom duration (months) - mean ± SD	91.6 ± 18.7
ALSFRS-r - mean ± SD	33.88 ± 5.05
Bulbar subscore (max 12) - mean ± SD	9.25 ± 2.24
ECAS - abnormal n (%)	16 (45.71%)
ECAS - mean ± SD	104.25 ± 18.57
FrSBe - abnormal n (%)	10 (28.57%)
HADS mean ± SD	8.25 (4.67)
Missing MRI data for volumetry/CTh/CERES/DWI/rs-fMRI	0/2/10/0/11

Abbreviations: CERES = CEREbellum Segmentation, CTh = cortical thickness, DWI = diffusion weighted imaging, ECAS = Edinburgh Cognitive and Behavioural ALS Screen, ELQ = emotional lability questionnaire, F = female, FrSBe = Frontal Systems Behavior Scale, HADS = Hospital Anxiety and Depression Scale, IQR = interquartile range, L = left-handed, M = male, PLS = primary lateral sclerosis, R = right(−handed), rs-fMRI = resting state functional magnetic resonance imaging, SD = standard deviation, y = years.

2.3. Genetics

All participating patients underwent whole exome sequencing, as previously described [16]. Protein altering variants in the exons and splice sites of 33 genes associated with ALS on the ALS online database [35] and 70 genes associated with hereditary spastic paraplegia (HSP) in the literature [36] were considered putative genetic variants. *C9orf72* hexanucleotide repeat expansion (HRE) status was evaluated using repeat-primed polymerase chain reaction (PCR) as described previously [37].

2.4. Study design

The main objective of the study was to investigate the neuroimaging correlates of the pseudobulbar affect (PBA) as measured by the emotional lability questionnaire [31]. Multiple MR sequences and their respective derived metrics were analysed: 1) structural T1-weigthed (T1w) data to estimate grey matter (GM) cortical thickness and volumes 2) diffusion-weighted imaging (DWI) to evaluate white matter (WM) microstructure integrity and 3) blood-oxygen-level-dependent (BOLD) signal acquired from resting-state functional MR imaging to assess functional connectivity (FC).

Two main analysis streams were pursued (Fig. 1); (1) a data-driven whole-brain exploratory arm without a priori anatomical hypotheses and (2) region-of-interest strategy based on prevailing pathophysiological theories. We started with the exploratory approach, i.e. we tested correlations between PBA scores and whole-brain data with no anatomical restrictions. The advantage of this approach is the potential to identify anatomical associations in an unbiased manner, which comes at the cost of reduced power given the increased numbers of statistical comparisons and thus elevated family-wise error (FWE) rate. While a variety of validated methods are available to control for FWE rate in

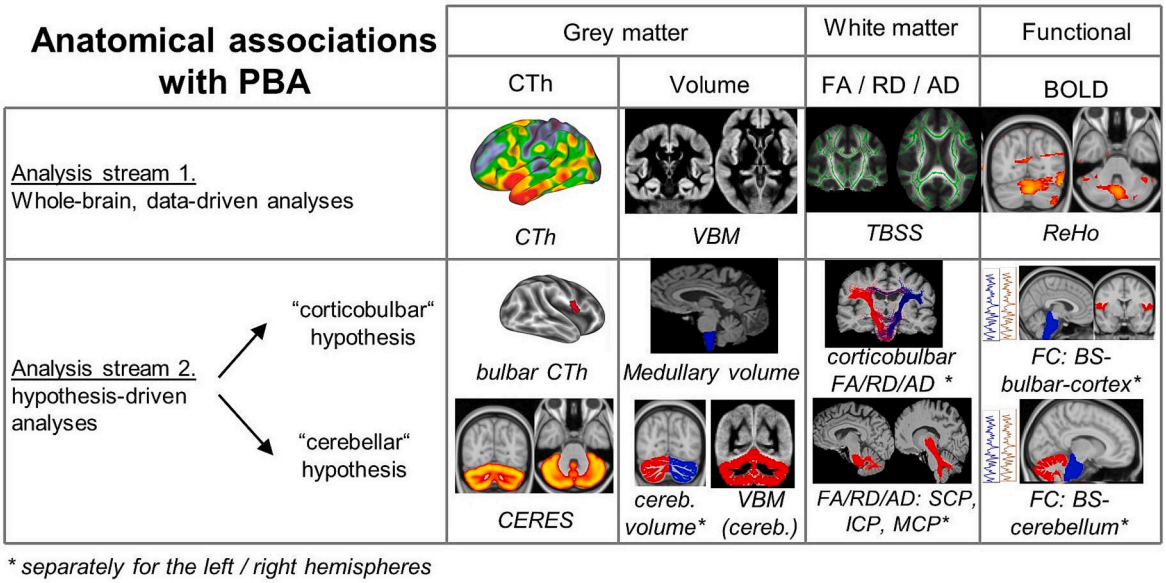

Fig. 1. The flowchart of the study design. Associations between pseudobulbar affect and multimodal neuroimaging metrics were analysed two main analysis streams (1) A data-driven, whole-brain, exploratory study without a priori anatomical hypotheses and (2) region-of-interest pipeline testing the "corticobulbar" and "cerebellar" theories of PBA. For each analysis streams, a panel of grey matter, white matter and functional imaging metrics were evaluated.
Abbreviations: AD = axial diffusivity, BOLD = blood-oxygen-level-dependent, BS = brainstem, cereb. = cerebellum, CERES = CEREbellar Segmentation, CTh = cortical thickness, FC = functional connectivity, FA = fractional anisotropy, ICP = inferior cerebellar peduncle, MCP = middle cerebellar peduncle, PBA = pseudobulbar affect, RD = radial diffusivity, ReHo = regional homogeneity, SCP = superior cerebellar peduncle, TBSS = tract-based spatial statistics, VBM = voxel-based morphometry.

neuroimaging, such as threshold-free cluster enhancement (TFCE) [38], we have also reviewed non-FWE-corrected outputs. In the second analysis stream, we followed a hypothesis-driven approach. In line with the two most common pathophysiological conceptualisation of PBA, the "corticobulbar bulbar hypothesis" and "cerebellar hypothesis", corticobulbar connectivity and cerebellar connectivity were specifically evaluated based on both structural and functional data. In each analysis stream, grey matter (GM), white matter (WM) and functional correlates of PBA were explored.

2.5. Data acquisition

All imaging data were uniformly acquired on the same 3 Tesla Philips Achieva scanner with an eight-channel receiver-only head coil. Three different MR pulse sequences were implemented to assess tissue types and connectivity. T1-weighted data were acquired with a 3D inversion recovery-prepared spoiled gradient recalled echo (IR-SPGR) sequence with the following settings: TR/TE = 8.5/3.9 ms, TI = 1060 ms, matrix size = 256 × 256 mm, 160 sagittal slices, spatial resolution: 1 mm isotropic, flip angle, (FA) = 8° and SENSE factor = 1.5. 2) Diffusion-weighted data were acquired with a spin-echo planar imaging (SE-EPI) pulse sequence with a 32-direction Stejskal-Tanner diffusion encoding scheme (b-values = 0/1100 s/mm^2) with the following main parameters: TR/TE = 7639/59 ms, matrix size = 245 × 245, 60 axial slices with no interslice gaps, spatial resolution = 2.5 mm isotropic, FA = 90°, SENSE factor = 2.5, dynamic stabilisation and spectral presaturation with inversion recovery (SPIR) fat suppression. Resting-state functional imaging (rsMRI) data were recorded with a T2-weighted EPI sequence to investigate BOLD signal fluctuations. 220 volumes were recorded with eyes closed implementing the following parameters: TR/TE = 2000 ms/35 ms, matrix size = 233 × 233, 30 axial slices, spatial resolution = 2.875 × 2.875 × 4 mm3, flip angle (FA) = 90°, SENSE factor = 2.5, pixel bandwidth ~1900, Hz/Px (with slight variations of up to 150 Hz/Px between subjects). For both analysis streams (Whole-brain and ROI), we retrieved GM, WM and BOLD neuroimaging metrics to evaluate anatomical associations with PBA scores. We describe the operationalisation and calculation of these metrics below, stratified by the analysis streams (Fig. 1). Relevant demographic variables including age, sex, handedness and years of education were recorded on the day of scanning to correct for potential confounds (Table 1). Relevant clinical data including the ECAS, HADS, ALSFRS-r, ELQ were collected within 2 weeks of the scan [30–32].

2.6. Analysis stream 1: whole-brain analyses

To explore whole-brain associations between grey matter morphometry and PBA, structural T1w data were pre-processed to derive estimates on both cortical thickness (CTh) and volumes. Whole-brain CTh maps were calculated using FreeSurfer's (version 7.3.2) automated pre-processing pipeline "recon-all" [39], which generates surface maps indicating CTh at each vertex. These data were converted into the CIFTI file format using the Ciftify toolbox to facilitate post-processing and visualization [40]. To explore GM alterations beyond CTh, voxel-based morphometry (VBM) was also performed using FMRIB's Software Library (FSL) version 6.0 [41] implementing the standard pipeline [42–44]. Associations between WM microstructure integrity metrics and PBA were investigated over the entire brain using FSL's tract-based spatial statistics (TBSS) [45]. DWI data were pre-processed within MRtrix3 (version 3.0.3) [46] to generate individual fractional anisotropy (FA), radial diffusivity (RD) and axial diffusivity (AD) maps as described previously [47,48]. In brief, pre-processing included de-noising [49,50], removal of Gibb's Ringing Artifacts [51], motion and eddy current correction [44] and bias field correction [52]. The pre-processed DW images were subsequently aligned to the high-resolution T1-weighted data. Resulting FA, RD and AD maps were fed into FSL's standard TBSS pipeline with registration to the FMRIB58-FA standard-space image, and nonlinear transformation to all subjects' FA, RD and AD images [45]. Whole-brain associations between BOLD signal fluctuations and PBA scores were explored as variations of regional homogeneity (ReHo) [53,54]. In brief, ReHo is a measure of functional network centrality and reflects synchronization of neural activity i.e. abnormal ReHo is regarded as proxy of altered neuronal

activity. For example, increased ReHo may suggest excessive activity of local neuronal populations, increased internal consistency and decreased synchronicity with other brain regions [55]. FSL's FEAT pipeline was used to pre-process BOLD data for ReHo including brain extraction, slice-time correction, and motion correction. The first five volumes were discarded to account for signal equilibrium. Correction of head-motion-related artifacts was added in a separate data preparation step using FSL's "AROMA" algorithm [56]. ReHo maps were computed within the Analysis of Functional NeuroImages (AFNI) suite (version 23.0.07) [57,58], using the "3dReHo" algorithm, which outputs voxel-wise maps of Kendall's W [59]. Correlations between the above whole-brain neuroimaging metrics and PBA scores (corrected for age, sex, handedness and years of education) were evaluated using FSL's "randomise" tool with 5000 permutations [60]. Associations between higher PBA scores and decreased radiological integrity i.e. decreased CTh, VBM-T1 signal, FA and increased AD, RD and ReHo were specifically investigated. We have subsequently reviewed both TFCE-corrected and uncorrected statistical maps evaluated at an alpha-threshold of $p \leq 0.05$.

2.7. Analysis stream 2: hypothesis-driven corticobulbar and cerebellar associations

The "corticobulbar" and "cerebellar" hypotheses were evaluated separately. The bulbar portion of the primary motor cortex was defined based on label "A4tl" of the Brainnetome atlas [61]. The medulla was first segmented using FreeSurfer's segmentBS tool [62]. We investigated GM-PBA associations based on medullary volumes and cortical thickness in the bulbar portion of the motor homunculus separately in right and left hemispheres using Matlab R2022b (The Mathworks, Natick, USA), tools from Workbench [63] and CoSMoMVPA [64]. GM variations in the cerebellum were operationalised as 1) the volume of the cerebellar hemispheres as per the "recon-all" output of the FreeSurfer pipeline, 2) VBM as described above, but restricted to a binary cerebellar mask and 3) cerebellar CTh maps using the software CEREbellar Segmenation, "CERES" [65], within volBrain [66]. CERES is a well-valided structural segmentation pipeline of the human cerebellum [67] which reliably generates voxelwise maps of cerebellar CTh for subsequent statistical interpretation.

WM-PBA associations for the "corticobulbar hypothesis" were operationalised as FA, RD and AD of the corticobulbar tract. The corticobulbar tract was defined as tracts linking the medulla and to the bulbar segment of the primary motor cortex (Fig. 2.), and accordingly, a fixed number ($N = 5000$) of corticobulbar streamlines were tracked between those two brain regions in MRtrix3. Tracking was performed separately for each hemisphere in each individual in native space. We estimated fibre orientation distributions (fODF) using the constrained spherical deconvolution model (CSD) [68,69] and estimated streamlines based on a probabilistic algorithm [70]. We then binarised these tractograms to extract the mean FA, RD and AD values per tract and subject using the previously calculated tensor maps. Similarly, WM-PBA associations for the "cerebellar hypothesis" were also operationalised as FA, RD and AD alterations in the five cerebellar peduncle tracts, the left (Lt) and right (Rt) superior cerebellar peduncles (SCP), the middle cerebellar peduncle (MCP) and left and right inferior cerebellar peduncles (ICP) (Fig. 2.). To identify these tracts, we used the TractSeg segmentation pipeline [71,72], which relies on a neural network algorithm to segment the WM tracts. TractSeg allows to estimate fODF using MRtrix3's CSD model, so that we could estimate cerebellar tracts analogously to the bulbar tract as outlined above. We binarised the cerebellar tracts and extracted mean FA, RD and AD values along the course of each tract.

Finally, BOLD-PBA associations were investigated based on functional connectivity (FC) between (1) the brainstem and the bulbar segment of the primary motor cortex to assess the "cortciobulbar hypothesis" and (2) between the brainstem and the cerebellum to test the "cerebellar hypothesis" separately in the left and right hemispheres. FC

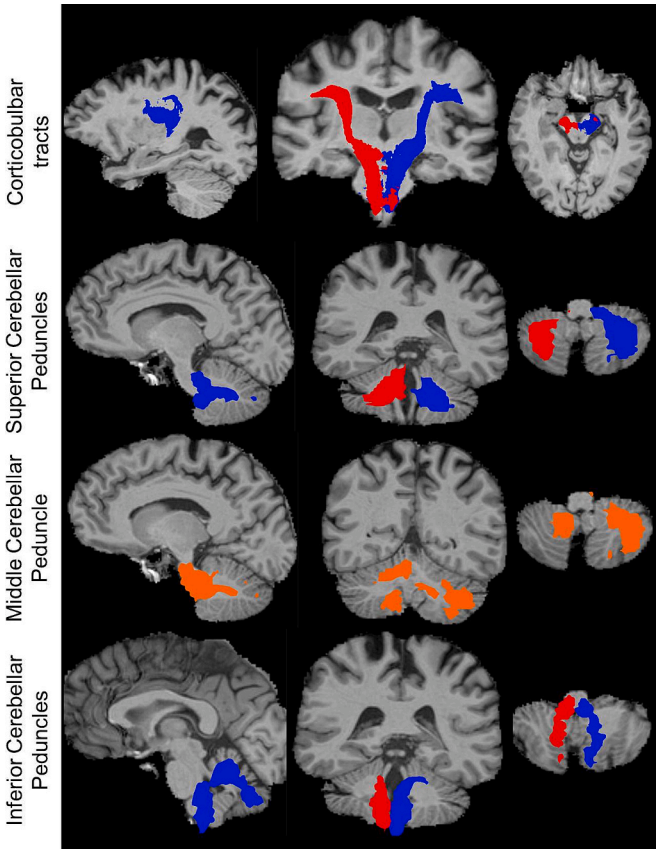

Fig. 2. Tractography for the corticobulbar tracts and cerebellar peduncles Representative sagittal, coronal and axial views are shown (left to right).

was calculated using the pre-processed BOLD data, extracting the mean time series of all voxels comprising the respective ROIs and computing pairwise Pearson's correlations between the pairwise ROIs within Matlab R 2022b.

Statistical associations between PBA scores and cerebellar VBM and CERES were investigated voxelwise using the relevant neuroimaging maps and design matrices, analogous to analysis stream 1, as described above. For the assessment of scalar metrics, such as ROI-wise volumes, CTh, FA, RD, AD and FC), we used a linear model, in which we modeled the specific neuroimaging metric as the independent and PBA scores as the dependent variable, accounting for the potential confounding effect of age, sex, handedness and years of education. These analyses were run within RStudio version 2023.03.0, using R Version 4.3.0 [73].

For the anatomical labelling of the relevant brain regions, we used the grey matter labels of the Harvard-Oxford cortical and subcortical structural atlases [74] and the MNI Cerebellar Atlas [75] and for the white matter, the JHU [76] and the XTRACT [77] atlases were utilised.

3. Results

3.1. Demographics

The demographic and clinical details of the study cohort are summarised in Table 1. As not every imaging modality was available for every patient, missing data were excluded from the respective analysis streams. All patients tested negative for *C9orf72* HRE as well as the panel of ALS and HSP associated genetic variants. ELQ scores did not show associations with ALSFRS-r ($p = 0.920117$), HADS-A, ($p = 0.47726$) HADS-D ($p = 0.8494$) or HADS-Total ($p = 0.64463$). The results of the correlation analyses between PBA and neuroimaging metrics are illustrated in Figs. 3–4, spanning form data-driven to hypothesis-driven

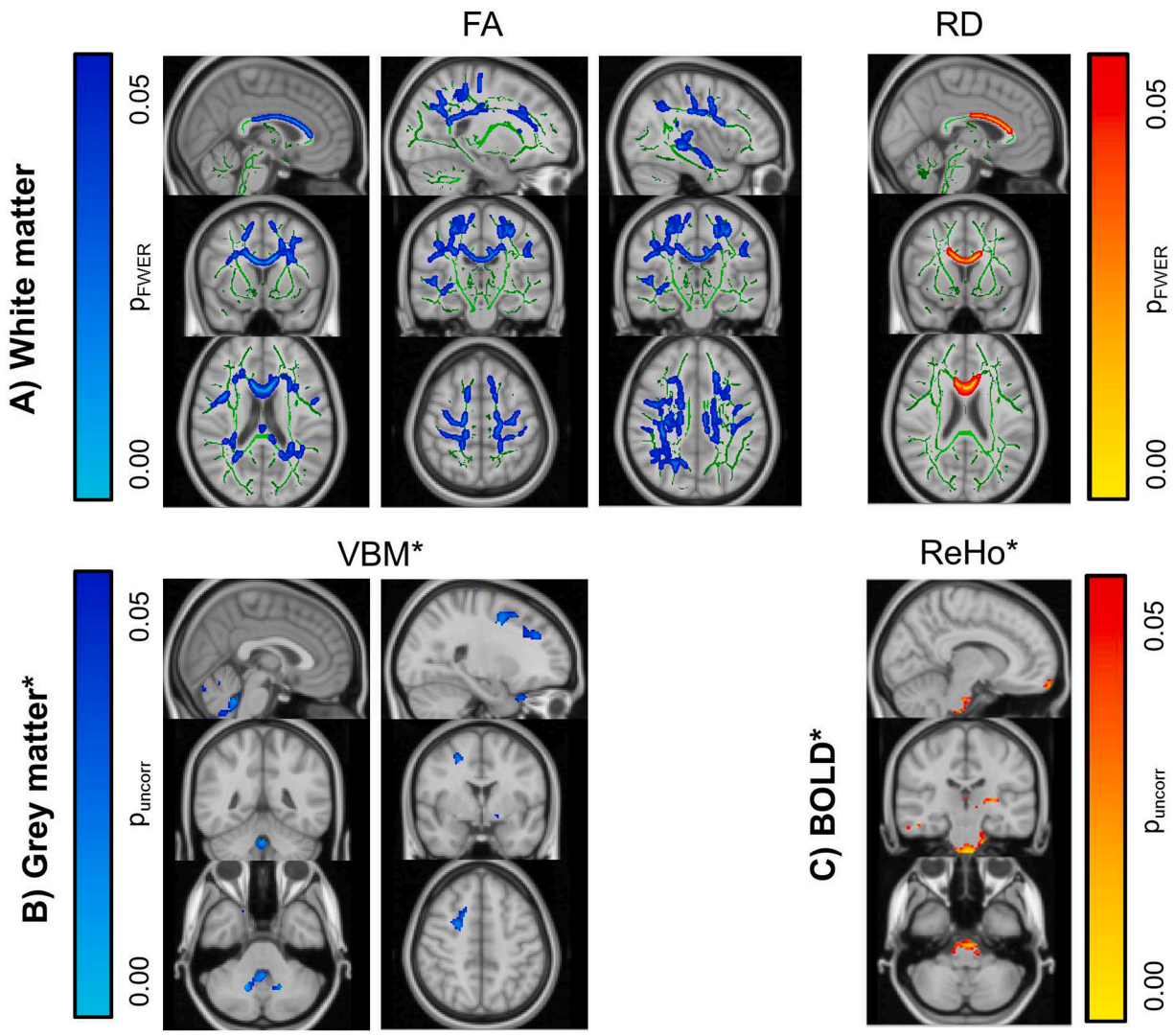

Fig. 3. Data-driven whole-brain analyses. The anatomical associations of pseudobulbar affect (ELQ) with white matter metrics (TBSS), grey matter indices (VBM and CTh anylses) and resting state functional MRI (BOLD - ReHo) to PBA (using ELQ scores) over the entire cerebrum were investigated. TBSS identified significant results after TFCE-correction for FA and RD (A), including significant correlations between more severe PBA and widespread FA reductions (CC, CST and association tracts) and RD increases in the CC. No voxels survived TFCE-correction for GM and BOLD analyses. Given the exploratory nature of the study, uncorrected p-maps thresholded at $p_{uncorr} \leq 0.05$ are also presented for VBM (B) and ReHo (C) revealing GM density reductions in the cerebellum and frontal cortical regions in association with higher ELQ (B) as well as increased uncorrected ReHo in the brainstem (C). CTh revealed on significant associations on corrected or uncorrected statistical maps.

* denotes FWE-uncorrected statistical maps, thresholded at $p_{uncorr} \leq 0.05$; otherwise maps are TFCE-corrected; cool colours indicate inverse correlations, hot colours denote direct correlations.

Voxel locations are provided in MNI152 2 mm standard space along with their original label names as per the relevant atlases provided in brackets: *Upper row, left to right* (labels according to JHU ICBM-DTI-81 WM labels atlas/XTRACT HCP Probabilistic Tract Atlases): 1) 91–138-93: Body of CC; 2) 67–107-127: right CST – also showing left CST, e.g. at 116–107-126; 3) 50–107-107: not labeled, suggestive of Corticobulbar Tract – also widespread parts of Arcuate/Superior Longitudinal/Middle Longitudinal/Inferior Longitudinal Fascicles; 4) 91–138-93: Body of Body of CC.

Lower row, left to right (labels according to Harvard-Oxford Cortical/Subcortical Atlases): 1) 44–39-18: Vermis; 2) 33–63-60: Precentral Gyrus – also showing Middle Frontal Gyurs at 33–78-51; 3) 40–51-14: Brainstem – also showing Frontal Pole, e.g. at 40–96-27, and left Putamen (60–51-38).

Abbreviations: AD = axial diffusivity, BOLD = blood-oxygen-level-dependent, CC = corpus callosum, CST = corticospinal tract, CTh = cortical thickness, DTI = diffusion tensor imaging, ELQ = emotional lability questionnaire, FA = fractional anisotropy, FWE(R) = family wise error (rate), GM = grey matter, ICBM = international consortium for brain mapping, HCP = human connectome project, JHU = Johns Hopkins University, PBA = pseudobulbar affect, RD = radial diffusivity, ReHo = regional homogeneity, TBSS = tract-based spatial statistics, TFCE = threshold-free cluster enhancement, VBM = voxel-based morphometry, WM = white matter, XTRACT = cross-species tractography

analyses. Comprehensive statistical details are provided in Tables 2 and 3.

3.2. Whole-brain analysis

In the first analysis stream, GM, WM and functional signal changes were considered over the entire brain in relation to PBA. Following TFCE-corrections, we found evidence that PBA is associated with WM changes in multiple anatomical regions (Fig. 3A). FA reductions correlated to increased ELQ scores in the corpus callosum (CC) and bilateral corticospinal tracts (CST), as well as in some association tracts. Increased RD was associated with higher ELQ scores, but only evident in the body of the CC. No significant associations were identified on AD TBSS analyses. For GM (as measured by VBM and CTh) and BOLD (as

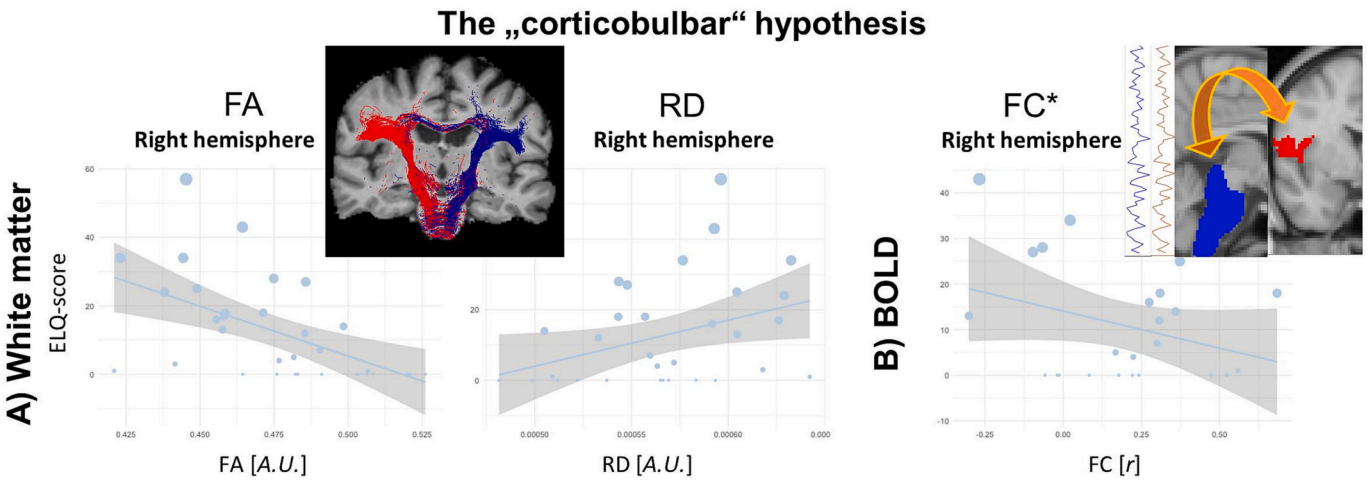

Fig. 4. The evaluation of the "corticobulbar hypothesis". Associations of pseudobulbar affect with white matter metrics (mean FA/RD/AD of the corticobulbar tract), grey matter indices (medullary volume, thickness of the bulbar motor cortex) and the functional connectivity between the brainstem and bulbar cortex (BOLD) were investigated. Significant associations were identified between the right-hemispheric corticobulbar tract and ELQ scores (A) including FA ($p = 0.006$) and RD ($p = 0.026$). For BOLD (B), a tendency ($p = 0.080$) for decreased FC between the brainstem and the bulbar segment of the primary motor cortex was identified. No associations with GM metrics reached significance at the alpha-level of $p < 0.05$. Statistical details are summarised in the main text and Table 2. * denotes tendency for significant association ($p < 0.10$).
Abbreviations: AD = axial diffusivity, BOLD = blood-oxygen-level-dependent, CTh = cortical thickness, ELQ = emotional lability questionnaire, FA = fractional anisotropy, FC = functional connectivity, FWE(R) = family wise error (rate), GM = grey matter, PBA = pseudobulbar affect, RD = radial diffusivity, WM = white matter

Table 2
Statistics of the "corticobulbar hypothesis", i.e. associations between corticobulbar metrics and PBA.

Neuroimaging metric	General linear model, testing main effect "neuroimaging metric"					
	Left hemisphere			Right hemisphere		
	Estimate	*t*-value	*p*-value	Estimate	*t*-value	*p*-value
Grey matter						
Medulla volume	−8.92e-7	−0.221	0.827	*n.a.*	*n.a.*	*n.a.*
Bulbar CTh	−4.25e-3	−1.036	0.310	−0.002	−0.593	0.558
White matter						
FA corticobulbar tract	−6.77e-4	−1.926	**0.065**+	−9.75e-4	−3.010	**0.006***
RD corticobulbar tract	1.04e−6	1.861	**0.074**+	1.25e-6	2.359	**0.026***
AD corticobulbar tract	3.25e-7	0.690	0.497	1.12e-7	0.248	0.806
BOLD						
FC brainstem-bulbar cortex	-6.22e-4	−0.165	0.871	−0.007	−1.853	**0.080**+

All statistics were derived from a GLM, investigating the main effect of the respective neuroimaging metrics (modeled as independent variable) on the dependent variable (ELQ scores). Potential confounding effects of age, sex, handedness and years of education were accounted for. One-sided testing scheme was used for all analyses, specifically testing the association between more severe PBA and decreased radiological integrity metrics i.e. decreased volume/CTh/FA/FC, increased RD/AD. As the medulla is a single structure, its volumetric analyses are only presented under the "left hemisphere" column. Bold font denotes statistical significance at an alpha level of $p \leq 0.05$; + denotes tendency for statistical significance at $p \leq 0.10$. Abbreviations: AD = axial diffusivity, BOLD = blood-oxygen-level-dependent, CTh = cortical thickness, ELQ = emotional lability questionnaire, FA = fractional anisotropy, FC = functional connectivity, GLM = general linear model, PBA = pseudobulbar affect, RD = radial diffusivity.

measured by ReHo) analyses, no voxels survived TFCE-corrections. However, given the exploratory nature of this first analysis stream, uncorrected *p*-maps were also reviewed thresholded at $p_{uncorr} \leq 0.05$, for both VBM (Fig. 3B) and ReHo (Fig. 3C) analyses. On these uncorrected maps, reduced T1w signal on VBM was associated with higher ELQ scores in the cerebellum and some frontal cortical regions. Increased ReHo in the brainstem was associated with increased ELQ scores. No associations were captured between PBA and CTh on whole-brain analyses, even when uncorrected *p*-maps were reviewed.

3.3. *"Corticobulbar hypothesis": Associations with structural and functional corticobulbar connectivity*

The whole-brain ReHo, VBM and TBSS findings were supportive of the "corticobulbar hypothesis", therefore this was specifically tested in dedicated ROI analyses. Fig. 4 summarises the significant results of this analysis stream and comprehensive statistical details are provided in Table 2. The pathology of the right-hemispheric corticobulbar tract showed particular associations with ELQ scores, as measured by FA reductions ($p = 0.006$) and RD increases ($p = 0.026$, Fig. 4A). For the left hemispheric corticobulbar tract, we only identified statistical trends for the analogous associations (FA: $p = 0.065$, RD: $p = 0.074$). Similar to the above correlations with structural corticobulbar connectivity metrics, functional measures also revealed associations. Lower functional connectivity (FC) between the bulbar segment of the right motor cortex and the medulla was associated with a trend of higher ELQ scores ($p = 0.080$, Fig. 4B). No associations were detected based on medullary volumes, cortical thickness of the bulbar segment of the motor cortex or axial diffusivity of the corticobulbar tracts.

Table 3
Statistics of the "cerebellar hypothesis", i.e. associations between cerebellar metrics and PBA.

Neuroimaging metric	General linear model, testing main effect "neuroimaging metric"					
	Left hemisphere			Right hemisphere		
	Estimate	*t*-value	*p*-value	Estimate	*t*-value	*p*-value
Grey matter						
Cerebellar cortical volume	−3.28e-5	−0.673	0.507	−1.73e-5	−0.379	0.707
Cerebellar cortical thickness	0.004	0.787	0.441	0.002	0.458	0.652
White matter						
Superior Cerebellar Peduncle (SCP)						
FA SCP	−2.71e-4	−0.972	0.340	−3.47e-4	−1.354	0.188
RD SCP	−1.80e-7	−0.369	0.715	2.56e-7	0.493	0.626
AD SCP	−1.37e-6	−2.059	**0.050**+	−7.45e-7	−1.032	0.312
Middle Cerebellar Peduncle (MCP)						
FA MCP	−3.63e-4	−1.106	0.279	*n.a.*	*n.a.*	*n.a.*
RD MCP	−9.43e-9	−0.015	0.988	*n.a.*	*n.a.*	*n.a.*
AD MCP	−9.76e-7	−1.292	0.208	*n.a.*	*n.a.*	*n.a.*
Inferior Cerebellar Peduncle (ICP)						
FA ICP	−4.43e-4	−1.021	0.317	−2.26e-4	−0.615	0.544
RD ICP	1.28e-7	0.157	0.876	3.84e-7	0.530	0.601
AD ICP	−9.00e-7	−0.862	0.396	5.84e-8	0.063	0.950
BOLD						
FC brainstem-cerebellum	0.002	0.309	0.761	−0.001	−0.242	0.812

All statistics were derived from a GLM, investigating the main effect of the respective neuroimaging metrics (modeled as independent variable) on the dependent variable (ELQ scores). Potential confounding effects of age, gender, handedness and years of education were accounted for. One-sided testing scheme was used for all analyses, specifically testing the association between more severe PBA and decreased radiological integrity metrics i.e. decreased volume/CTh/FA/FC, increased RD/AD. As the MCP was evaluated as a single structure, its analyses are only presented under the "left hemisphere" column. Bold"+" denotes tendency for statistical significance at $p \leq 0.10$. Abbreviations: AD = axial diffusivity, BOLD = blood-oxygen-level-dependent, CTh = cortical thickness, ELQ = emotional lability questionnaire, FA = fractional anisotropy, FC = functional connectivity, GLM = general linear model, MCP = Middle Cerebellar Peduncle, ICP = Inferior Cerebellar Peduncle, PBA = pseudobulbar affect, RD = radial diffusivity, SCP = Superior Cerebellar Peduncle, WM = white matter.

3.4. The cerebellar hypothesis: no supporting radiological findings identified

In our final analysis stream, we have evaluated a panel of structural and functional cerebellar metrics, but no associations were identified with pseudobulbar symptoms. Statistical details are provided in Table 3. Cerebellar grey matter volume and thickness did not show associations with ELQ scores. Similarly, voxelwise cerebellar GM correlations did reach significance either on VBM or for CTh following FWE-corrections. However, the inspection of the FWE-uncorrected *p*-maps for VBM and CTh revealed T1w signal reduction (VBM) and CTh reduction (CERES) of the vermis in association with increased ELQ. Similarly, none of the structural WM connectivity metrics (FA, RD, AD) of the cerebellar peduncles (Lt/Rt SCP, MCP, Lt/Rt ICP) yielded statistically relevant associations with PBA. Only a trend of association was identified between higher ELQ scores and higher AD in the left SCP ($p = 0.0501$). In terms of functional connectivity, neither left- nor right-hemispheric FC decreases were identified between the brainstem and the cerebellum in association with PBA on BOLD analyses.

4. Discussion

In accordance with the classical pathophysiological model of PBA, our findings implicate the structural and functional disconnection of the bulbar segment of the motor cortex and the brainstem. Our initial data-driven, whole-brain analyses revealed voxelwise correlations along the descending corticospinal/corticobulbar tracts. Uncorrected morphometric analyses also revealed a trend for association with cerebellar grey mater metrics. In line with the two most popular pathophysiological models, cortico-bulbar and cerebellar hypotheses were specifically evaluated in post hoc region-of-interest analyses.

The integration of research findings in PBA is hindered by differences in terminology, diagnostic criteria and screening practices in different geographical regions and in different neurological conditions. Despite the definition of specific thresholds on various PBA rating scales, the presence of PBA is unlikely to binary (present or not) but likely to be along a spectrum of symptom severity which may be progressive in certain conditions [78]. While the 1969 *Poeck's* criteria [79] centres primarily on context-inappropriate emotional manifestations, more recent criteria are more permissive, recognising presentations across the whole spectrum of PBA [2,80]. The Revised "involuntary emotional expression disorder" (IEED) criteria [2] encompass episodes that are merely disproportionate to the emotive stimulus and are different from the patient's emotional reactivity prior to disease onset. Supportive clinical features, such as outbursts of anger, smiling, yawning are increasingly considered [4,80–82]. Given the spectrum of manifestations we did not stratify patients into symptomatic or asymptomatic individuals based on pre-defined thresholds on the ELQ scales, but used their absolute ELQ score values in correlation models. Our clinical findings (Table 1.) also underscore that the degree of pseudobulbar affect is independent from anxiety, depression and physical disability and not a direct correlate of the above disease dimensions. This is in line with the conceptualisation of PBA as mood incongruent episodes of emotional manifestations and also consistent with studies in ALS where typically PBA cannot be linked directly to underlying depression [3,14,25,83,84]. The most commonly used screening scales include the 1993 Pathological laughing and crying scale (PLACS) [85], the self-reported Center for Neurologic Study-Lability Scale (CNS-LS) [86,87] which has been extensively utilised in recent pharmacological trials [88–91]. The "emotional lability questionnaire" (ELQ) has also been consistently utilised in MND. It takes symptoms into to up to four weeks prior to screening into account, which helps to ascertain patients with experience frequent symptoms [92,93]. ELQ also evaluates the caregiver's views on the patients PBA, but in MND, the patient and caregiver scores are typically concordant [92]. While a multitude of validated instruments exist to appraise the severity of PBA, the specific quality of life (QoL) ramifications of PBA are relatively understudied [4,83], despite evidence that it not only impacts on the social life of affected patients [94] but also on caregivers [95]. Even though multiple therapeutic approaches exist, these are not always effective and divergent strategies are typically used in different conditions. In neurovascular conditions, selective serotonin reuptake inhibitors (SSRIs) are typically trialled first [82], but tricyclic antidepressants (TCAs) are also widely utilised [85]. In MND, amitriptyline [96] and duloxetine [97] are often

used as first-line therapies. Memantine is sometimes used in Alzheimer's disease. Since 2010, dextromethorphan/quinidine (Dx/Q) is increasingly prescribed and randomised, double-blinded studies have confirmed its efficiency in ALS [90]. Despite the multitude of therapeutic options, achieving full symptom control can be challenging and often a combination of drugs are prescribed.

In our study we have exclusively included patients with primary lateral sclerosis. PLS is a low-incidence neurodegenerative condition with one of the highest rates of pseudobulbar affect in any neurological condition, making it an ideal cohort to study to likely underpinnings of this clinical syndrome. Radiologically, PLS is classically associated with motor cortex, corticospinal tract and corpus callosum degeneration [17,98–100], but extra-pyramidal involvement is also increasingly recognised [16,101]. While there are considerable radiological similarities between ALS and PLS [102], and PBA is also prevalent in ALS, PLS is associated with a considerably better prognosis than ALS. It has been previously stipulated that frontotemporal pathology may play a role in the aetiology of PBA, but as demonstrated in our cohort, there are no direct associations noted on any of the whole- brain, data-driven analyses between frontotemporal integrity and ELQ scores. Our voxelwise and vertex wise, grey- and white matter analyses did not capture significant associations between frontotemporal metrics and PBA.

The strong association noted between PBA and corticobulbar tract integrity may have broader clinical and diagnostic ramifications in motor neuron diseases and potentially in other neurological syndromes. Compared to the plethora of routinely evaluated pathological upper motor neuron (UMN) signs in the limbs; Babinski, Oppenheim, Gordon, Chaddock, Hoffmann's, Tromner's etc. there is a paucity or reliable bulbar UMN signs. The jaw-jerk (masseter reflex) is often equivocal early in neurodegenerative conditions, when it may be difficult to elicit and reliably interpret. Similarly spastic dysarthria may be difficult to confidently ascertain unless reviewed by expert speech pathologist or trained speech and language therapists [103]. Accordingly, in the correct context, PBA may be an excellent clinical indicator of corticobulbar tract involvement or cortico-medullary disconnection. This in turn may have diagnostic implications, particularly in ALS, where concomitant LMN signs may be readily identified on clinical or neurophysiological assessment [103]. As the quantitative analyses of corticobulbar tract integrity based on DWI, fMRI, or transcranial magnetic stimulation (TMS) are time-consuming, expensive and many MND patients do not tolerate MRI scanning [104], the presence of marked PBA may be interpreted as evidence of corticobulbar tract pathology.

Our whole-brain and targeted cerebellar analyses did not reach significance, although a trend of association was identified between higher ELQ scores and higher AD in the left SCP ($p = 0.0501$). Notwithstanding our findings in PLS, cerebellar involvement has been previously linked to PBA in ALS [12,13] and relatively selective cerebellar signatures have been consistently described in various motor neuron disease phenotypes [105–108]. While frank ataxia is seldom observed in PLS or ALS, subclinical cerebellar involvement is thought to contribute to neuropsychological deficits, exacerbate dysarthria, worsen gait impairment, and potentially impact on dysphagia or respiratory patterns [106,109–112].

From a methodological perspective, the multimodal approach adopted in our study permits the appraisal of specific measures. There is a relatively strong concordance between structural and function imaging metrics in highlighting structural and functional disconnection between brain regions. Structural connectivity metrics however captured statistically significant association both in whole-brain and ROI analyses. We have investigated there diffusivity metrics, FA, AD and RD, but only FA and RD alterations were associated with clinical measures in corticobulbar tracts. In the cerebellar analysis stream however, a trend of association was identified between higher ELQ scores and higher AD in the left SCP. These observations confirm the merits of a multimodal imaging protocol including a panel of structural and functional measures and more importantly, the systematic assessment of multiple diffusivity indices. Cortical thickness is one of the most commonly assessed radiological metric in MND, in no small part, due to the excellent semi-automated pipelines. Interestingly, in our study measures of PBA did not reveal associations with focal grey matter atrophy neither on the cerebral vertex or in the cerebellum. This confirms that specific symptoms may not be solely driven by unifocal anatomical changes, rather stem from the dysfunction of neuronal networks with multiple cortical, subcortical and white matter components [113–117]. Connectivity analyses should therefore be incorporated in exploratory studies aiming to decipher the underpinnings of specific symptoms. We also note the relative symmetry of our findings; imaging metrics of bilateral structures were evaluated in the left and right hemispheres separately and resulted in concordant findings. We also note that none of the patients carried the *C9orf72* HRE which would have introduced a potential confound given the unique clinical and radiological correlates of that genotype [37,118,119].

This study is not without limitations. While comprehensive genetic and clinical assessments were performed, we have only evaluated a relatively small cohort of patients. A single PBA battery was administered, and a cross-sectional study design implemented. Given the evidence of progressive radiological changes in PLS [120,121], this approach precludes the characterisation of worsening PBA over time. Our findings may be specific to PLS and alternative pathomechanisms may contribute to PBA in other conditions. Notwithstanding these limitations, our imaging study confirms the association between cortico-medullary disconnection and pseudobulbar affect.

5. Conclusions

Pseudobulbar affect in PLS is associated with structural and functional cortico-medullary disconnection. Additional cerebellar components may also play a role and it is likely that the aetiology of PBA is multifactorial with the involvement of multiple cerebral networks.

Funding

This study was sponsored by the Spastic Paraplegia Foundation (SPF). Professor Bede is also supported by the Health Research Board (HRB EIA-2017-019 & JPND-Cofund-2-2019-1), the Irish Institute of Clinical Neuroscience (IICN), the EU Joint Programme – Neurodegenerative Disease Research (JPND), the Andrew Lydon Scholarship, The Hayes Family Charitable Fund and the Iris O'Brien Foundation. RLMcL, MAD and JCH are supported by the MND Association (898–792) and Science Foundation Ireland (17/CDA/4737).

Authors contribution

The manuscript was drafted by MT, ELT, PB. Study conceptualisation: MT, ELT, WFS, EF, PB. Clinical assessments: EF, OH, PB. MR data processing and analyses: MT, ELT, PB. Genetics analyses: RLMcL, MAD, JCH.

Ethics approval

This study was approved by the Ethics (Medical Research) Committee—Beaumont Hospital, Dublin, Ireland (IRB).

Declaration of Competing Interest

The authors have no financial or non-financial interests to disclose.

Data availability statement

Group-level outputs, statistical maps, and post-hoc statistics can be requested from the corresponding author. Individual patient clinical and neuroimaging data cannot be made available due to institutional regulations and departmental policies.

Acknowledgements

We are most thankful for the participation of each patient, and we also thank all patients who expressed interest in this research study but were unable to participate for medical or logistical reasons. We also express our gratitude to the caregivers and families of PLS patients for facilitating attendance at our neuroimaging centre. Without their generosity this study would have not been possible.

References

[1] H. Oppenheim, Textbook of Nervous Diseases for Physicians and Students by Professor H. Oppenheim of Berlin, English Trans-Lation by Alexander Bruce, T. N. Foulis Publisher, London, Edinburgh, 1911.
[2] J.L. Cummings, D.B. Arciniegas, B.R. Brooks, et al., Defining and diagnosing involuntary emotional expression disorder, CNS Spectr. 11 (S6) (2006) 1–7.
[3] N.T. Olney, M.S. Goodkind, C. Lomen-Hoerth, et al., Behaviour, physiology and experience of pathological laughing and crying in amyotrophic lateral sclerosis, Brain 134 (12) (2011) 3455–3466.
[4] F. Ahmed, J. Murphy, C. Lomen-Hoerth, Utility of a new pseudobulbar questionnaire (PBAQ) for ALS, Ann. Neurol. 68 (2010) S23–S24.
[5] M.K. Floeter, R. Katipally, M.P. Kim, et al., Impaired corticopontocerebellar tracts underlie pseudobulbar affect in motor neuron disorders, Neurology 83 (7) (2014) 620–627.
[6] D. Wynn, R. Kaye, A. Hepner, Impact of pseudobulbar affect on health and QoL, Ann. Neurol. 68 (2010) S12.
[7] S.A.K. Wilson, Original Papers. Some Problems in Neurology s1–4(16), 1924, pp. 299–333.
[8] J. Parvizi, S.W. Anderson, C.O. Martin, et al., Pathological laughter and crying: a link to the cerebellum, Brain 124 (Pt 9) (2001) 1708–1719.
[9] C.J. Stoodley, J.D. Schmahmann, Evidence for topographic organization in the cerebellum of motor control versus cognitive and affective processing, Cortex 46 (7) (2010) 831–844.
[10] J. Parvizi, K.L. Coburn, S.D. Shillcutt, et al., Neuroanatomy of pathological laughing and crying: a report of the American neuropsychiatric association committee on research, J. Neuropsychiatr. Clin. Neurosci. 21 (1) (2009) 75–87.
[11] T. Murai, H. Barthel, J. Berrouschot, et al., Neuroimaging of serotonin transporters in post-stroke pathological crying, Psychiatry Res. 123 (3) (2003) 207–211.
[12] F. Christidi, E. Karavasilis, P. Ferentinos, et al., Investigating the neuroanatomical substrate of pathological laughing and crying in amyotrophic lateral sclerosis with multimodal neuroimaging techniques, Amyotr. Later. Scler. Frontotemporal. Degener. 19 (1–2) (2018) 12–20.
[13] F. Trojsi, F. Di Nardo, G. D'Alvano, et al., Resting state fMRI analysis of pseudobulbar affect in amyotrophic lateral sclerosis (ALS): motor dysfunction of emotional expression, Brain Imag. Behav. 17 (1) (2023) 77–89.
[14] P. Bede, E. Finegan, Revisiting the pathoanatomy of pseudobulbar affect: mechanisms beyond corticobulbar dysfunction, Amyotr. Later. Scler. Frontotemporal. Degener. 19 (1–2) (2018) 4–6.
[15] N. Thakore, E. Pioro, Prevalence, associations and course of depression in ALS: observations from a large cohort, Amyotr. Later. Scler. Frontotemp. Degen. 15 (2014) 55–56.
[16] E. Finegan, S.L.H. Shing, R.H. Chipika, et al., Extra-motor cerebral changes and manifestations in primary lateral sclerosis, Brain Imag. Behav. 15 (5) (2021) 2283–2296.
[17] E. Finegan, R.H. Chipika, S. Li Hi Shing, et al., The clinical and radiological profile of primary lateral sclerosis: a population-based study, J. Neurol. 266 (11) (2019) 2718–2733.
[18] P.F. Pradat, E. Bernard, P. Corcia, et al., The French national protocol for Kennedy's disease (SBMA): consensus diagnostic and management recommendations, Orphanet J. Rare Dis. 15 (1) (2020) 90.
[19] Li Hi Shing, R.H. Chipika, E. Finegan, et al., Post-polio syndrome: more than just a lower motor neuron disease, Front. Neurol. 10 (2019) 773.
[20] Li Hi Shing, J. Lope, R.H. Chipika, et al., Extra-motor manifestations in post-polio syndrome (PPS): fatigue, cognitive symptoms and radiological features, Neurol. Sci. 42 (11) (2021) 4569–4581.
[21] M.V. Lebouteux, J. Franques, R. Guillevin, et al., Revisiting the spectrum of lower motor neuron diseases with snake eyes appearance on magnetic resonance imaging, Eur. J. Neurol. 21 (9) (2014) 1233–1241.
[22] G. Querin, M.M. El Mendili, T. Lenglet, et al., The spinal and cerebral profile of adult spinal-muscular atrophy: a multimodal imaging study, Neuroimage Clin. 21 (2019), 101618.
[23] G. Querin, T. Lenglet, R. Debs, et al., The motor unit number index (MUNIX) profile of patients with adult spinal muscular atrophy, Clin. Neurophysiol. 129 (11) (2018) 2333–2340.
[24] G. Querin, T. Lenglet, R. Debs, et al., Development of new outcome measures for adult SMA type III and IV: a multimodal longitudinal study, J. Neurol. 268 (5) (2021) 1792–1802.
[25] E. Finegan, R.H. Chipika, S. Li Hi Shing, et al., Pathological crying and laughing in motor neuron disease: pathobiology, screening, intervention, Front. Neurol. 10 (2019) 260.
[26] T. Burke, M. Elamin, P. Bede, et al., Discordant performance on the 'Reading the mind in the Eyes' test, based on disease onset in amyotrophic lateral sclerosis, Amyotr. Later. Scler. Frontotemporal. Degener. 17 (7–8) (2016) 467–472.
[27] R.H. Chipika, F. Christidi, E. Finegan, et al., Amygdala pathology in amyotrophic lateral sclerosis and primary lateral sclerosis, J. Neurol. Sci. 417 (2020), 117039.
[28] F. Christidi, E. Karavasilis, G. Velonakis, et al., The clinical and radiological Spectrum of hippocampal pathology in amyotrophic lateral sclerosis, Front. Neurol. 9 (2018) 523.
[29] M.R. Turner, R.J. Barohn, P. Corcia, et al., Primary lateral sclerosis: consensus diagnostic criteria, J. Neurol. Neurosurg. Psychiatry 91 (4) (2020) 373–377.
[30] S. Abrahams, J. Newton, E. Niven, et al., Screening for cognition and behaviour changes in ALS, Amyotr. Later. Scler. Frontotemporal. Degener. 15 (1–2) (2014) 9–14.
[31] I.C. Newsom-Davis, S. Abrahams, L.H. Goldstein, et al., The emotional lability questionnaire: a new measure of emotional lability in amyotrophic lateral sclerosis, J. Neurol. Sci. 169 (1–2) (1999) 22–25.
[32] J.M. Cedarbaum, N. Stambler, E. Malta, et al., The ALSFRS-R: a revised ALS functional rating scale that incorporates assessments of respiratory function. BDNF ALS study group (phase III), J. Neurol. Sci. 169 (1–2) (1999) 13–21.
[33] M. Pinto-Grau, T. Burke, K. Lonergan, et al., Screening for cognitive dysfunction in ALS: validation of the Edinburgh cognitive and Behavioural ALS screen (ECAS) using age and education adjusted normative data, Amyotr. Later. Scler. Frontotemporal. Degener. 18 (1–2) (2017) 99–106.
[34] J.O. Carvalho, R.E. Ready, P. Malloy, et al., Confirmatory factor analysis of the frontal systems behavior scale (FrSBe), Assessment 20 (5) (2013) 632–641.
[35] O. Abel, A. Shatunov, A.R. Jones, et al., Development of a smartphone app for a genetics website: the amyotrophic lateral sclerosis online genetics database (ALSoD), JMIR mHealth uHealth 1 (2) (2013) e18.
[36] S. Klebe, G. Stevanin, C. Depienne, Clinical and genetic heterogeneity in hereditary spastic paraplegias: from SPG1 to SPG72 and still counting, Rev. Neurol. (Paris) 171 (6–7) (2015) 505–530.
[37] S. Byrne, M. Elamin, P. Bede, et al., Cognitive and clinical characteristics of patients with amyotrophic lateral sclerosis carrying a C9orf72 repeat expansion: a population-based cohort study, Lancet Neurol. 11 (3) (2012) 232–240.
[38] S.M. Smith, T.E. Nichols, Threshold-free cluster enhancement: addressing problems of smoothing, threshold dependence and localisation in cluster inference, NeuroImage 44 (1) (2009) 83–98.
[39] B. Fischl, FreeSurfer, Neuroimage 62 (2) (2012) 774–781.
[40] E.W. Dickie, A. Anticevic, D.E. Smith, et al., Ciftify: a framework for surface-based analysis of legacy MR acquisitions, Neuroimage 197 (2019) 818–826.
[41] M. Jenkinson, C.F. Beckmann, T.E.J. Behrens, et al., FSL, NeuroImage 62 (2) (2012) 782–790.
[42] G. Douaud, S. Smith, M. Jenkinson, et al., Anatomically related grey and white matter abnormalities in adolescent-onset schizophrenia, Brain 130 (Pt 9) (2007) 2375–2386.
[43] C.D. Good, I.S. Johnsrude, J. Ashburner, et al., A voxel-based morphometric study of ageing in 465 normal adult human brains, Neuroimage 14 (1 Pt 1) (2001) 21–36.
[44] S.M. Smith, M. Jenkinson, M.W. Woolrich, et al., Advances in functional and structural MR image analysis and implementation as FSL, Neuroimage 23 (Suppl. 1) (2004) S208–S219.
[45] M. Bach, F.B. Laun, A. Leemans, et al., Methodological considerations on tract-based spatial statistics (TBSS), NeuroImage 100 (2014) 358–369.
[46] J.D. Tournier, R. Smith, D. Raffelt, et al., MRtrix3: a fast, flexible and open software framework for medical image processing and visualisation, NeuroImage 202 (2019), 116137.
[47] M.C. McKenna, M. Tahedl, A. Murad, et al., White matter microstructure alterations in frontotemporal dementia: phenotype-associated signatures and single-subject interpretation, Brain Behav 12 (2) (2022) e2500.
[48] M. Tahedl, A. Murad, J. Lope, et al., Evaluation and categorisation of individual patients based on white matter profiles: single-patient diffusion data interpretation in neurodegeneration, J. Neurol. Sci. 428 (2021), 117584.
[49] J. Veraart, E. Fieremans, D.S. Novikov, Diffusion MRI noise mapping using random matrix theory, Magn. Reson. Med. 76 (5) (2016) 1582–1593.
[50] J. Veraart, D.S. Novikov, D. Christiaens, et al., Denoising of diffusion MRI using random matrix theory, Neuroimage 142 (2016) 394–406.
[51] E. Kellner, B. Dhital, V.G. Kiselev, et al., Gibbs-ringing artifact removal based on local subvoxel-shifts, Magn. Reson. Med. 76 (5) (2016) 1574–1581.
[52] N.J. Tustison, B.B. Avants, P.A. Cook, et al., N4ITK: improved N3 bias correction, IEEE Trans. Med. Imaging 29 (6) (2010) 1310–1320.
[53] Y. Zhu, M. Huang, Y. Zhao, et al., Local functional connectivity of patients with acute and remitting multiple sclerosis: a Kendall's coefficient of concordance- and coherence-regional homogeneity study, Medicine (Baltimore) 99 (43) (2020), e22860.
[54] Y. Zang, T. Jiang, Y. Lu, et al., Regional homogeneity approach to fMRI data analysis, Neuroimage 22 (1) (2004) 394–400.
[55] T. Wu, X. Long, Y. Zang, et al., Regional homogeneity changes in patients with Parkinson's disease, Hum. Brain Mapp. 30 (5) (2009) 1502–1510.
[56] R.H.R. Pruim, M. Mennes, D. van Rooij, et al., ICA-AROMA: a robust ICA-based strategy for removing motion artifacts from fMRI data, Neuroimage 112 (2015) 267–277.
[57] R.W. Cox, AFNI: software for analysis and visualization of functional magnetic resonance neuroimages, Comput. Biomed. Res. 29 (3) (1996) 162–173.
[58] R.W. Cox, J.S. Hyde, Software tools for analysis and visualization of fMRI data, NMR Biomed. 10 (4–5) (1997) 171–178.

[59] P.A. Taylor, Z.S. Saad, FATCAT: (an efficient) functional and Tractographic connectivity analysis toolbox, Brain Connect 3 (5) (2013) 523–535.
[60] A.M. Winkler, G.R. Ridgway, M.A. Webster, et al., Permutation inference for the general linear model, Neuroimage 92 (100) (2014) 381–397.
[61] L. Fan, H. Li, J. Zhuo, et al., The human Brainnetome atlas: a new brain atlas based on connectional architecture, Cereb. Cortex 26 (8) (2016) 3508–3526.
[62] J.E. Iglesias, K. Van Leemput, P. Bhatt, et al., Bayesian segmentation of brainstem structures in MRI, Neuroimage 113 (2015) 184–195.
[63] D.S. Marcus, J. Harwell, T. Olsen, et al., Informatics and data mining tools and strategies for the human connectome project, Front. Neuroinform. 5 (2011) 4.
[64] N.N. Oosterhof, A.C. Connolly, J.V. Haxby, CoSMoMVPA: multi-modal multivariate pattern analysis of neuroimaging data in Matlab/GNU octave, Front. Neuroinform. 10 (2016) 27.
[65] J.E. Romero, P. Coupé, R. Giraud, et al., CERES: a new cerebellum lobule segmentation method, Neuroimage 147 (2017) 916–924.
[66] J.V. Manjón, P. Coupé, volBrain: an online MRI brain volumetry system, Front. Neuroinform. 10 (2016) 30.
[67] A. Carass, J.L. Cuzzocreo, S. Han, et al., Comparing fully automated state-of-the-art cerebellum parcellation from magnetic resonance images, Neuroimage 183 (2018) 150–172.
[68] J.D. Tournier, C.H. Yeh, F. Calamante, et al., Resolving crossing fibres using constrained spherical deconvolution: validation using diffusion-weighted imaging phantom data, Neuroimage 42 (2) (2008) 617–625.
[69] J.D. Tournier, F. Calamante, A. Connelly, Robust determination of the fibre orientation distribution in diffusion MRI: non-negativity constrained super-resolved spherical deconvolution, Neuroimage 35 (4) (2007) 1459–1472.
[70] J.D. Tournier, F. Calamante, A. Connelly, Improved probabilistic streamlines tractography by 2nd order integration over fibre orientation distributions, in: Proceedings of the International Society for Magnetic Resonance in Medicine (ISMRM), 2010, p. 18.
[71] J. Wasserthal, P. Neher, K.H. Maier-Hein, TractSeg - fast and accurate white matter tract segmentation, NeuroImage 183 (June) (2018) 239–253.
[72] J. Wasserthal, P.F. Neher, D. Hirjak, et al., Combined tract segmentation and orientation mapping for bundle-specific tractography, Med. Image Anal. 58 (2019), 101559.
[73] R Core Team, R: A language and environment for statistical computing. Vienna, Austria, URL, http://www, 2014. R-project. org, 2015.
[74] N. Makris, J.M. Goldstein, D. Kennedy, et al., Decreased volume of left and total anterior insular lobule in schizophrenia, Schizophr. Res. 83 (2–3) (2006) 155–171.
[75] J. Diedrichsen, J.H. Balsters, J. Flavell, et al., A probabilistic MR atlas of the human cerebellum, Neuroimage 46 (1) (2009) 39–46.
[76] K. Hua, J. Zhang, S. Wakana, et al., Tract probability maps in stereotaxic spaces: analyses of white matter anatomy and tract-specific quantification, Neuroimage 39 (1) (2008) 336–347.
[77] S. Warrington, K.L. Bryant, A.A. Khrapitchev, et al., XTRACT - standardised protocols for automated tractography in the human and macaque brain, Neuroimage 217 (2020), 116923.
[78] W.M. Sauvé, Recognizing and treating pseudobulbar affect, CNS Spect. 21 (S1) (2016) 37–43.
[79] K. Poeck, Pathophysiology of emotional disorders associated with brain damage, in: P. Vinken, G. Bruyn (Eds.), Handbook of Clinical Neurology, North Holland, 1969, pp. 3–343.
[80] A. Miller, H. Pratt, R.B. Schiffer, Pseudobulbar affect: the spectrum of clinical presentations, etiologies and treatments, Expert. Rev. Neurother. 11 (7) (2011) 1077–1088.
[81] O. Ghaffar, L. Chamelian, A. Feinstein, Neuroanatomy of pseudobulbar affect: a quantitative MRI study in multiple sclerosis, J. Neurol. 255 (3) (2008) 406–412.
[82] S. Choi-Kwon, S.W. Han, S.U. Kwon, et al., Fluoxetine treatment in poststroke depression, emotional incontinence, and anger proneness: a double-blind, placebo-controlled study, Stroke 37 (1) (2006) 156–161.
[83] Z.L. Adirim, J. Caga, E. Ramsey, et al., I can't help that i look sad: the experience of emotional lability in the ALS patient and caregiver, Amyotr. Later. Scler. Frontotemp. Degen. 16 (2015) 34.
[84] K. Lonergan, T. Burke, M. Pinto-Grau, et al., Emotional lability in ALS: delineating the relationship between lability, psychological status, cognition, and behavior, Amyotr. Later. Scler. Frontotemp. Degen. 17 (2016) 273.
[85] R.G. Robinson, R.M. Parikh, J.R. Lipsey, et al., Pathological laughing and crying following stroke: validation of a measurement scale and a double-blind treatment study, Am. J. Psychiatry 150 (2) (1993) 286–293.
[86] S.R. Moore, L.S. Gresham, M.B. Bromberg, et al., A self report measure of affective lability, J. Neurol. Neurosurg. Psychiatry 63 (1) (1997) 89–93.
[87] R.A. Smith, J.E. Berg, L.E. Pope, et al., Measuring pseudobulbar affect in ALS, Amyotr. Lateral Scler. Other Motor Neuron Disord. 5 (Suppl. 1) (2004) 99–102.
[88] F.M. Hammond, D.N. Alexander, A.J. Cutler, et al., PRISM II: an open-label study to assess effectiveness of dextromethorphan/quinidine for pseudobulbar affect in patients with dementia, stroke or traumatic brain injury, BMC Neurol. 16 (1) (2016).
[89] E.P. Pioro, B.R. Brooks, J. Cummings, et al., Dextromethorphan plus ultra low-dose quinidine reduces pseudobulbar affect, Ann. Neurol. 68 (5) (2010) 693–702.
[90] B.R. Brooks, R.A. Thisted, S.H. Appel, et al., Treatment of pseudobulbar affect in ALS with dextromethorphan/quinidine: a randomized trial, Neurology 63 (8) (2004) 1364–1370.
[91] H.S. Panitch, R.A. Thisted, R.A. Smith, et al., Randomized, controlled trial of dextromethorphan/quinidine for pseudobulbar affect in multiple sclerosis, Ann. Neurol. 59 (5) (2006) 780–787.
[92] A. Palmieri, S. Abrahams, G. Soraru, et al., Emotional lability in MND: relationship to cognition and psychopathology and impact on caregivers, J. Neurol. Sci. 278 (1–2) (2009) 16–20.
[93] I.C. Newsom-Davis, S. Abrahams, L.H. Goldstein, et al., The emotional lability questionnaire: a new measure of emotional lability in amyotrophic lateral sclerosis, J. Neurol. Sci. 169 (1–2) (1999) 22–25.
[94] J. Colamonico, A. Formella, W. Bradley, Pseudobulbar affect: burden of illness in the USA, Adv. Ther. 29 (9) (2012) 775–798.
[95] L.H. Goldstein, L. Atkins, S. Landau, et al., Predictors of psychological distress in carers of people with amyotrophic lateral sclerosis: a longitudinal study, Psychol. Med. 36 (6) (2006) 865–875.
[96] A. Szczudlik, A. Slowik, B. Tomik, The effect of amitriptyline on the pathological crying and other pseudobulbar signs, Neurol. Neurochir. Pol. 29 (5) (1995) 663–674.
[97] P. Ferentinos, T. Paparrigopoulos, M. Rentzos, et al., Duloxetine for pathological laughing and crying in amyotrophic lateral sclerosis, Eur. Neuropsychopharmacol. 19 (2009) S409.
[98] E.P. Pioro, M.R. Turner, P. Bede, Neuroimaging in primary lateral sclerosis, Amyotr. Later. Scler. Frontotemporal. Degener. 21 (sup1) (2020) 18–27.
[99] P. Bede, P.F. Pradat, J. Lope, et al., Primary lateral sclerosis: clinical, radiological and molecular features, Rev. Neurol. (Paris) 178 (3) (2022) 196–205.
[100] M. Tahedl, E.L. Tan, S.L.H. Shing, et al., Not a benign motor neuron disease: longitudinal imaging captures relentless motor connectome disintegration in primary lateral sclerosis, Eur. J. Neurol. 30 (5) (2023) 1232–1245.
[101] E. Finegan, S. Li Hi Shing, R.H. Chipika, et al., Widespread subcortical grey matter degeneration in primary lateral sclerosis: a multimodal imaging study with genetic profiling, Neuroimage Clin. 24 (2019), 102089.
[102] E. Finegan, R.H. Chipika, S.L.H. Shing, et al., Primary lateral sclerosis: a distinct entity or part of the ALS spectrum? Amyotr. Later. Scler. Frontotemporal. Degener. 20 (3–4) (2019) 133–145.
[103] Y. Yunusova, E.K. Plowman, J.R. Green, et al., Clinical measures of bulbar dysfunction in ALS, Front. Neurol. 10 (2019) 106.
[104] P. Bede, G. Querin, P.F. Pradat, The changing landscape of motor neuron disease imaging: the transition from descriptive studies to precision clinical tools, Curr. Opin. Neurol. 31 (4) (2018) 431–438.
[105] P. Bede, R.H. Chipika, F. Christidi, et al., Genotype-associated cerebellar profiles in ALS: focal cerebellar pathology and cerebro-cerebellar connectivity alterations, J. Neurol. Neurosurg. Psychiatry 92 (11) (2021) 1197–1205.
[106] R.H. Chipika, G. Mulkerrin, P.F. Pradat, et al., Cerebellar pathology in motor neuron disease: neuroplasticity and neurodegeneration, Neural Regen. Res. 17 (11) (2022) 2335–2341.
[107] E. Finegan, W.F. Siah, S. Li Hi Shing, et al., Cerebellar degeneration in primary lateral sclerosis: an under-recognized facet of PLS, Amyotr. Later. Scler. Frontotemporal. Degener. (2022) 1–12.
[108] S. Li Hi Shing, A. Murad, J. Lope, et al., Cerebellar remodelling decades after spinal cord insult: neuroplasticity in poliomyelitis survivors, J. Integr. Neurosci. 21 (2) (2022) 65.
[109] M. Abidi, G. de Marco, A. Couillandre, et al., Adaptive functional reorganization in amyotrophic lateral sclerosis: coexisting degenerative and compensatory changes, Eur. J. Neurol. 27 (1) (2020) 121–128.
[110] M. Abidi, G. de Marco, F. Grami, et al., Neural correlates of motor imagery of gait in amyotrophic lateral sclerosis, J. Magn. Reson. Imaging 53 (1) (2021) 223–233.
[111] M. Abidi, P.F. Pradat, N. Termoz, et al., Motor imagery in amyotrophic lateral sclerosis: an fMRI study of postural control, Neuroimage Clin. 35 (2022), 103051.
[112] M. Feron, A. Couillandre, E. Mseddi, et al., Extrapyramidal deficits in ALS: a combined biomechanical and neuroimaging study, J. Neurol. 265 (9) (2018) 2125–2136.
[113] E. Verstraete, M.R. Turner, J. Grosskreutz, et al., Mind the gap: the mismatch between clinical and imaging metrics in ALS, Amyotr. Later. Scler. Frontotemporal. Degener. 16 (7–8) (2015) 524–529.
[114] P. Bede, Deciphering neurodegeneration: a paradigm shift from focality to connectivity, Neurology 89 (17) (2017) 1758–1759.
[115] M. Proudfoot, P. Bede, M.R. Turner, Imaging cerebral activity in amyotrophic lateral sclerosis, Front. Neurol. 9 (2018) 1148.
[116] R.H. Chipika, E. Finegan, S. Li Hi Shing, et al., "switchboard" malfunction in motor neuron diseases: selective pathology of thalamic nuclei in amyotrophic lateral sclerosis and primary lateral sclerosis, Neuroimage Clin. 27 (2020), 102300.
[117] J.M. Meier, H.K. van der Burgh, A.D. Nitert, et al., Connectome-based propagation model in amyotrophic lateral sclerosis, Ann. Neurol. 87 (5) (2020) 725–738.
[118] S. Li Hi Shing, M.C. McKenna, W.F. Siah, et al., The imaging signature of C9orf72 hexanucleotide repeat expansions: implications for clinical trials and therapy development, Brain Imag, Behav. 15 (5) (2021) 2693–2719.
[119] P. Bede, R.H. Chipika, E. Finegan, et al., Progressive brainstem pathology in motor neuron diseases: imaging data from amyotrophic lateral sclerosis and primary lateral sclerosis, Data Brief. 29 (2020), 105229.
[120] M. Tahedl, S. Li Hi Shing, E. Finegan, et al., Propagation patterns in motor neuron diseases: individual and phenotype-associated disease-burden trajectories across the UMN-LMN spectrum of MNDs, Neurobiol. Aging 109 (2021) 78–87.
[121] M. Tahedl, S. Li Hi Shing, E. Finegan, et al., Imaging data reveal divergent longitudinal trajectories in PLS, ALS and poliomyelitis survivors: group-level and single-subject traits, Data Brief. 39 (2021), 107484.

Glossary

AD: axial diffusivity
AFNI: Analysis of Functional NeuroImages
ALS: amyotrophic lateral sclerosis
ALSFRS-r: revised amyotrophic lateral sclerosis functional rating scale
ANOVA: analysis of variance
AUC: area under the curve
BA: "bulbar asymptomatic"- patients with spinal onset disease without bulbar manifestations
BrS: Brainstem shape
BOLD: blood-oxygen-level-dependent signal
C9orf72: chromosome 9 open reading frame 72
CBT: corticobulbar tract
CC: corpus callosum
CERES: CEREbellum Segmentation
CoSMoMVPA: Multi-Modal Multivariate Pattern Analysis
CSD: constrained spherical deconvolution
CST: corticospinal tract
CT: cortical thickness
CTh: cortical thickness
DTI: diffusion tensor imaging
DWI: diffusion weighted imaging
ECAS: Edinburgh Cognitive and Behavioural ALS Screen
EMM: estimated marginal mean
EL: emotional lability
ELQ: emotional lability questionnaire
EPI: echo-planar imaging
FA: fractional anisotropy
FC: functional connectivity
FLAIR: fluid-attenuated inversion recovery
fMRI: functional MRI
fODF: estimated fibre orientation distributions
FOV: field of view
FrSBe: Frontal Systems Behavior Scale
FSL: FMRIB's Software Library
FTD: frontotemporal dementia
FWE: familywise error
GM: grey matter
HADS: Hospital Anxiety and Depression Scale
HARDI: high angular resolution diffusion-weighted imaging
HC: healthy control
HCP: Human Connectome Project
HRE: hexanucleotide repeat expansion
HSP: hereditary spastic paraplegia
ICBM: International Consortium for Brain Mapping
ICP: inferior cerebellar peduncle
IEED: involuntary emotional expression disorder
IR-SPGR: inversion recovery prepared spoiled gradient recalled echo
IQR: interquartile range
IR-TSE: inversion recovery turbo spin echo sequence
JHU: Johns Hopkins University
LH: left hemisphere
LL: lower limb
LMN: lower motor neuron
Lt: Left
M1: primary motor cortex
MCP: middle cerebellar peduncle
ML: machine-learning
MND: Motor neuron disease
MNI152: Montreal Neurological Institute 152 standard space
MRS: magnetic resonance spectroscopy
MS: multiple sclerosis
MSA-C: multiple system-atrophy-cerebellar type
MV: medullary volume
NODDI: neurite orientation dispersion and density imaging
PBA: pseudobulbar affect
PCL: pathological crying and laughing
PCR: polymerase chain reaction
PLS: Primary lateral sclerosis
PM: premotor area
PMC: primary motor cortex
PUMS: Penn Upper Motor Neuron Score
QC: quality control
ReHo: regional homogeneity
RH: right hemisphere
RD: Radial diffusivity
ROI: region of interest
rsFMRI: resting-state functional MRI
Rt: right
SBMA: spinal-bulbar muscular atrophy
SC: structural connectivity
SCP: superior cerebellar peduncle
SD: standard deviation
SE-EPI: spin-echo echo planar imaging
SENSE: sensitivity Encoding
SMA: supplementary motor area
SPIR: spectral presaturation with inversion recovery
SSRIs: selective serotonin reuptake inhibitors
T: Tesla
T1w: T1-weighted imaging
TBI: traumatic brain injury
TBSS: tract-based spatial statistics
TCA: tricyclic antidepressants
TFCE: threshold-free cluster enhancement
TE: echo time
TI: inversion time
TIV: total intracranial volume
TMS: transcranial magnetic stimulation
TR: repetition time
Tukey HSD test: Tukey's Honest Significant Difference test
UL: upper limb
UMN: upper motor neuron
WES: whole exome sequencing
WM: white matter
XTRACT: cross-species tractography